

# Raman-induced localization in Kerr waveguide arrays

Dima Cheskis,<sup>1,3</sup> Yoav Linzon,<sup>1</sup> Iftach Ilisar,<sup>1</sup> Shimshon Bar-Ad,<sup>1,\*</sup> and Hagai S. Eisenberg<sup>2</sup>

<sup>1</sup>*School of Physics and Astronomy, Faculty of Exact Sciences, Tel-Aviv University, Tel Aviv 69978, Israel*

<sup>2</sup>*Racah Institute of Physics, Hebrew University of Jerusalem, Jerusalem 91904, Israel*

<sup>3</sup>*Present address: Department of Chemistry, Technion, Haifa 32000, Israel*

\*Corresponding author: shimshon@post.tau.ac.il

Received February 6, 2007; revised July 11, 2007; accepted July 18, 2007;  
posted July 24, 2007 (Doc. ID 82674); published August 13, 2007

We show that during the spatiotemporal compression in a periodic Kerr waveguide array, stimulated Raman scattering can effectively balance the effects of self-phase modulation, diffraction, and group-velocity dispersion, eliminating collapse and breakup over a wide range of input powers and leading to stable propagation in a single site. © 2007 Optical Society of America  
OCIS codes: 190.4420, 190.5530.

The stable propagation of localized excitations is a central and active field of nonlinear optics [1]. Media with composite structures, such as periodic weakly coupled waveguide arrays (WGAs), have intriguing nonlinear localized excitations that have been extensively studied in recent years [2–7]. While low-power excitations evolve as extended waves in the transmission spectrum (TS) bands of a structure, high-power nonlinear localized excitations reside in the TS gaps, opposing diffraction or group-velocity dispersion (GVD) and forming spatial or temporal solitons. Multidimensional  $1+d$  localized excitations, occurring simultaneously in  $d=2,3$  dimensions, have also been extensively studied for both multispatial [2,3,8,9] and spatiotemporal [4,5,10–13] cases. Importantly, when time is a canonical dimension, its dynamics are not analogous to a conjugate space dimension. This stems from the fact that temporal localization of a pulse approaching collapse (induced by self-phase modulation (SPM) in combination with the proper sign of GVD [1]) is accompanied by higher-order effects. These effects include high-order dispersion, saturation of the Kerr nonlinearity, and Stokes Raman shift of the central carrier frequency [14], the latter making the Kerr nonlinearity kernel time dependent. The resulting changes in the temporal pulse shape and power density also have direct consequences to the spatial dynamics [11–13].

Recalling our previous experiments on spatiotemporal localization (STL) [5,12,13], performed on planar glass waveguides with anomalous GVD and a focusing Kerr nonlinearity, Figure 1 shows the output width as a function of the input peak power, following propagation of  $\sim 60$  fs input pulses through a 3 cm long silica slab and through a 3 cm long planar WGA. The WGA consists of weakly coupled single-mode-doped channels, buried in a pure silica substrate (for sample details see [5,13]). In both cases, the input is a  $30 \mu\text{m}$  wide beam, corresponding to an excitation of a single site of the WGA. In both geometries, at powers below a critical value  $I_c$  (different in each geometry), both the space and time dimensions exhibit simultaneous compression. However, beyond  $I_c$  the dynamics are fundamentally different. In the slab

case simultaneous spatial, spectral, and temporal breakup of the beam occurs [11,13,15] as collapse is being avoided due to high-order effects. In contrast, the WGA exhibits a localized excitation that locks to a single site (Fig. 1) [5], evading breakup and collapse even at powers an order of magnitude higher than  $I_c$ . So far the origin of the strong STL has remained elusive, since (as shown below) this sustained stability against collapse cannot be explained by the standard physical picture.

Here we explain how the strong STL results from a balance between the effects of SPM (which induces spatiotemporal collapse), stimulated Raman scattering (SRS, which effectively resists collapse through the chromatic dispersion of the waveguide mode), and the linear effects of dispersion and diffraction in the periodic structure. This is, to the best of our knowledge, the first demonstration of Raman-induced localization in WGAs.

The  $1+2$  spatiotemporal dynamics of the electric field  $E(x,t,z)$  in the WGA is modeled using the nonlinear Schrödinger equation (NLSE),

$$i \frac{\partial E}{\partial z} = -\frac{1}{2k} \frac{\partial^2 E}{\partial x^2} + \hat{d}(E) + k \frac{n_2}{n_0(x)} E \hat{r}(|E|^2), \quad (1)$$

where  $k$  is the wavenumber,  $n_0(x)$  is the position-dependent refractive index,  $n_2 > 0$  is the focusing Kerr coefficient,  $\hat{d}(E) = \sum_{n=2}^4 (1/n!) \beta_n (\partial^n E / \partial t^n)$  is the dispersion operator, taken up to the fourth order, and

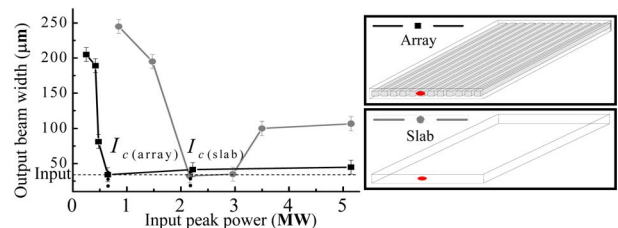


Fig. 1. (Color online) Experimental results for 60 fs pulses focused into glass waveguides with anomalous GVD and a focusing Kerr nonlinearity. Squares, 3 cm long waveguide array; circles, 3 cm long slab waveguide. The input beam width corresponds to excitation of a single array site.

$\hat{r}(|E|^2) = \int_{-\infty}^t R(t-\tau) |E(\tau)|^2 d\tau$  is the Kerr nonlinearity operator, combined with the effect of SRS.  $n_0(x)$  is an effective refractive index, taking into account the confinement in the vertical ( $y$ ) direction. The Raman time-kernel  $R(t')$  consists of the sum of instantaneous (electronic) and delayed (vibrational) responses [14],  $R(t') = f_{inst} \delta(t') + (1 - f_{inst}) h_R(t')$ , where  $f_{inst}$  is the fraction of the response that is electronic, and  $h_R(t')$  is an oscillatory function that decays with a picosecond time constant [14]. In the 1+1 case, where the GVD is normal ( $\beta_2 > 0$ ), there is broadening of the pulse during propagation. The noninstantaneous part of the Kerr nonlinearity can then be neglected, and a separation of variables is possible, the temporal dynamics being unimportant for nonlinear processes. Moreover, when considering weakly coupled WGAs, a discrete nearest-neighbor version of the spatial NLSE is usually sufficient, and provides good approximations for the dynamics [6,7]. However, temporal compression is expected to produce collapse [5] (or at least self-focusing within a single waveguide), features that do not exist in the discrete model where maximum focusing means that all the power is localized in a single site. In this case, the continuous Eq. (1) must be employed.

We first solve the standard NLSE that does not include variation of parameters [Eq. (1)]. Our numerical code, implemented on a CRAY supercomputer, uses the split-step technique [14]. The domain is a  $1024 \times 1024$  grid with total sizes of  $500 \mu\text{m}$  in  $x$  and  $500 \text{fs}$  in  $t$ . This corresponds to a space domain resolution of four points within a single site and eight points between adjacent sites of the WGA in the  $n_0(x)$  grid. For numerical convergence, particularly in the sensitive region of maximum STL,  $z$  is propagated in subwavelength resolution. The initial excitation is taken as a Gaussian of the form  $E(x, t, z=0) = E_0 \exp[-x^2/2w_0^2 - t^2/2t_0^2]$ , with  $w_0 = 25 \mu\text{m}$  and  $t_0 = 60 \text{fs}$ . The values for GVD ( $\beta_2 < 0$ ) and high-order dispersion ( $\beta_3, \beta_4 \ll \beta_2$ ) are taken from the literature [14] for  $\lambda_0 = 1520 \text{nm}$ . Figure 2 shows the output  $x-t$  profiles for different input power densities ( $I = |E_0|^2$ ), following 3.5 cm long propagation (slightly longer than the experimental value, chosen in order to monitor the dynamics in the vicinity of the output facet). The well-known discrete diffraction pattern [6,7] is obtained at low powers [Fig. 2(a)], and a local-

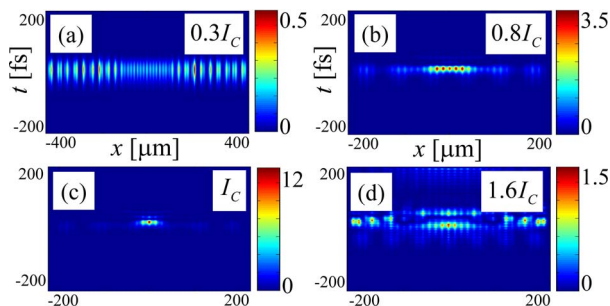


Fig. 2. (Color online) Simulated spatiotemporal contour plots for 3.5 cm propagation of Eq. (1) with different input power densities.  $I_C = 0.3 \text{MW}$ . The colorbars next to each panel indicate the fluence in  $\text{MW}/\text{m}^2$  units.

ized excitation forms as  $I_C$  is approached [Figs. 2(b) and 2(c)]. While the localization is sustained at slightly higher powers, a further increase of power results in an abrupt breakup of the beam [Fig. 2(d)], in contradiction to the data of Fig. 1. This spatial breakup is accompanied by a splitting of the original pulse to several pulses in the time domain. Therefore the basic model presented above cannot account for the strong STL that is sustained over an order of magnitude of optical power levels. Figure 3 illustrates the high-power propagation maps in space (integrated over time) [Fig. 3(a)], in time (integrated over space) [Fig. 3(b)], and in the spectral domain [Fig. 3(c)]. It is evident that the breakup occurs at the same distance where the redshift of the spectrum is most pronounced.

The spectral redshift during STL is a key feature of the dynamics, which generally affects all other parameters in Eq. (1), including the dispersion coefficients and the Raman time kernel. We have found that the most important contribution arises from the fact that the single-waveguide mode is wavelength dependent and is less localized for longer wavelengths. This modal change occurs in the WGA dimension  $x$ , and also in the vertical (confined) dimension  $y$ , which imposes a change of the effective propagation constant and thus the effective refractive index. The broadening of the single-waveguide mode results in an increased nearest-neighbor coupling, equivalent to increased diffraction. These changes are effectively introduced into the simulation through a modification of the refractive index during propagation  $n_0(x) \rightarrow n_0(x, z)$ . An unrelated effect, not captured in Eq. (1), is a lower effective power density between the waveguides, resulting from a weaker vertical mode confinement. This affects only the nonlinear term in Eq. (1), and cancels in the others. To take this into account,  $|E(x)|^2$  in the nonlinear term can be replaced with  $|\tilde{E}(x)|^2$ , where  $\tilde{E}$  is an effective amplitude. The two corrections can be incorporated into the following, modified, NLSE:

$$i \frac{\partial E}{\partial z} = \dots + k \frac{n_2}{n_0(x, z)} E \hat{r}(|\tilde{E}(x)|^2). \quad (2)$$

Equation (2) is difficult to solve, since it requires a 3D simulation. However, note that in the spirit of the 2D approximation, the modulation of the effective amplitude  $\tilde{E}$  can be imitated by introducing an  $x$ -dependent nonlinear index,  $n_2(x)$ . In our implementation the variation of  $n_2(x)$  is taken to be sinusoidal with a 33% modulation depth:  $n_2(x) = n_{2(0)}/4 [\cos(2\pi x/d) + 3]$ , where  $d$  is the waveguide's

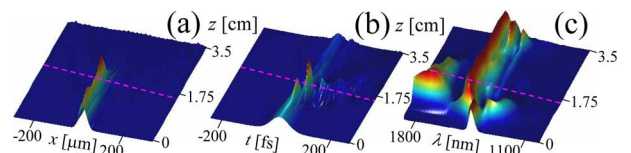


Fig. 3. (Color online) Propagation maps of the (a) spatial, (b) temporal, and (c) spectral dimensions for the basic simulation with a  $I = 1.6 I_C$  excitation [see Fig. 2(d)].

width. The final simulation, which includes both effects, is represented by the following equation:

$$i \frac{\partial E}{\partial z} = \dots + k \frac{n_2(x)}{n_0(x,z)} E \hat{r}(|E|^2). \quad (3)$$

Equation (3) is implemented in steps, such that in each step the index profile  $n_0(x)$  is modified according to the spectral shift of the beam in the preceding step, and the values of  $n_0(x)$  correspond to the propagation constants of the single-waveguide mode (calculated using the known spectral dispersion of silica [14]). The results are summarized in Fig. 4. Panel (a) shows a spatial propagation map of a high-power beam obtained with the basic simulation, Eq. (1). In this case the beam breaks up at  $z \approx 0.7$  cm. Application of the  $n_0(x,z)$  correction greatly stabilizes the beam [Fig. 4(b)]. When the  $n_2(x)$  correction is also applied, the beam is stabilized to a single site [Fig. 4(c), Eq. (3)]. The variation of the mode index that we obtained from the simulation is plotted in Fig. 4(d). We have also verified that when only the nonlinear correction is applied, the beam breaks up. Thus our simulations show that the combination of the two effects extends the regime of stability well beyond  $I_c$ . While computer resources limited our ability to simulate propagation at intensities above  $2I_c$ , we expect this stability to be sustained even at higher powers, provided that the corrections are applied in sufficiently small steps. These results can be interpreted as follows: at a single-site excitation there are two competing nonlinearities, the Kerr nonlinearity (that tends to squeeze the waveguide mode through self-focusing), and the Raman nonlinearity (that expands the waveguide mode, and is therefore equivalent to self-broadening) [Fig. 4(e)]. The balance of these nonlinearities leads to stable propagation without breakup, and is robust as both effects grow with

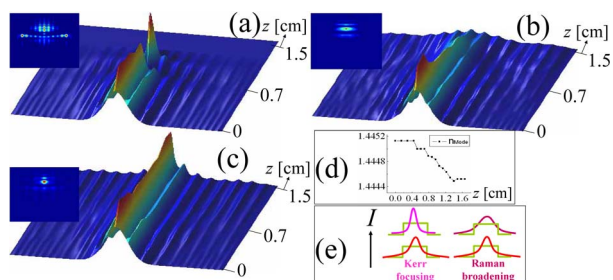


Fig. 4. (Color online) (a)–(c) Spatial propagation maps and output spatiotemporal profiles (insets) of a  $I=2I_c$  beam: (a) basic simulation [Eq. (1)]; (b) with a  $n_0(x,z)$  dynamic correction; (c) with both  $n_0(x,z)$  and  $n_2(x)$  corrections [Eq. (3)]; (d) single-waveguide refractive index as a function of  $z$  obtained from (b); (e) illustration of the Raman-assisted localization in a single site.

power. We conclude that in the presence of the periodic modulation of the WGA, the Raman effect and high-order GVD stabilize the soliton in the spatial dimension. It is known that the same effects usually have the opposite result, i.e., fission of the soliton [15]. Indications of such fission in the temporal dimension are indeed observed [see the insets of Figs. 4(a)–4(c)].

In conclusion, we have demonstrated that a strong spatiotemporal localization, robust with increasing input power, cannot be explained using the standard NLSE, but originates from the Raman-induced Stokes redshift of the spectrum, which causes self-broadening. This counteracts the Kerr-induced self-focusing of the waveguide mode that individually leads to the breakup of the beam. Inhomogeneity of the vertical confinement further enhances the localization.

This research was supported by the Israel Science Foundation through grants 8006/03 and 944/05.

## References

1. R. W. Boyd, *Nonlinear Optics*, 2nd ed. (Academic, 2002).
2. J. W. Fleischer, M. Segev, N. K. Efremidis, and D. N. Christodoulides, *Nature* **422**, 147 (2003).
3. D. Neshev, E. Ostrovskaya, Yu. Kivshar, and W. Krolikowski, *Opt. Lett.* **28**, 710 (2003).
4. A. B. Aceves, G. G. Luther, C. De Angelis, A. M. Rubenchik, and S. K. Tyrutsky, *Phys. Rev. Lett.* **75**, 73 (1995).
5. D. Cheskis, S. Bar-Ad, R. Morandotti, J. S. Aitchison, H. S. Eisenberg, Y. Silberberg, and D. Ross, *Phys. Rev. Lett.* **91**, 223901 (2003).
6. D. N. Christodoulides and R. I. Joseph, *Opt. Lett.* **13**, 794 (1988).
7. H. S. Eisenberg, Y. Silberberg, R. Morandotti, A. R. Boyd, and J. S. Aitchison, *Phys. Rev. Lett.* **81**, 3383 (1998).
8. M. Soljačić, S. Sears, and M. Segev, *Phys. Rev. Lett.* **30**, 4851 (1998).
9. C.-C. Jeng, M.-F. Shih, K. Motzek, and Y. Kivshar, *Phys. Rev. Lett.* **92**, 043904 (2004).
10. P. Di Trapani, G. Valiulis, A. Piskarskas, O. Jedrkiewicz, J. Trull, C. Conti, and S. Trillo, *Phys. Rev. Lett.* **91**, 093904 (2003).
11. A. V. Yulin, D. V. Skryabin, and P. St. J. Russell, *Opt. Lett.* **30**, 525 (2005).
12. H. S. Eisenberg, R. Morandotti, Y. Silberberg, S. Bar-Ad, D. Ross, and J. S. Aitchison, *Phys. Rev. Lett.* **87**, 043902 (2001).
13. Y. Linzon, I. Ilsar, D. Cheskis, R. Morandotti, J. S. Aitchison, and S. Bar-Ad, *Phys. Rev. E* **72**, 066607 (2005).
14. G. P. Agrawal, *Nonlinear Fiber Optics*, 3rd ed. (Academic, 2001).
15. A. V. Husakou and J. Herrmann, *Phys. Rev. Lett.* **87**, 203901 (2001).